Oligo(*p*-phenyleneethynylene) (OPE) Molecular Wires: Synthesis and Length Dependence of Photoinduced Charge Transfer in OPEs with Triarylamine and Diaryloxadiazole End Groups

Katharine E. Linton, Mark A. Fox, Lars-Olof Pålsson* and Martin R. Bryce*

Department of Chemistry, Durham University, Durham DH1 3LE, UK

E-mails: m.r.bryce@durham.ac.uk; lars-olof.palsson@durham.ac.uk

Keywords: Oligo(phenyleneethynylene) / triarylamine / oxadiazole / donor-acceptor system / charge-transfer / photoinduced / molecular wire

Abstract: The systematic synthesis, photophysical, electrochemical and computational studies are reported on an extended series of triphenylamine-[C≡C-1,4-$C_6H_2(OR)_2$]$_n$-C≡C-diphenyl-1,3,4-oxadiazole dyad molecules (the OR groups are at 2,5 positions of the *para*-phenylene ring and R = C_6H_{13}; n = 0-5, compounds **1**, **2**, **3**, **4** and **5**, respectively). Related molecules with identical end groups, triphenylamine-C≡C-1,4-$C_6H_2(OR)_2$-C≡C-triphenylamine (R = C_6H_{13}; **6**) and diphenyl-1,3,4-oxadiazole-[C≡C-$C_6H_2(OR)_2$]$_2$-C≡C-diphenyl-1,3,4-oxadiazole (R = C_6H_{13}; **7**) were also studied. These D-B-A **1-5**, D-B-D **6** and A-B-A **7** (D = electron donor; B = bridge; A = electron acceptor) systems were synthesized using palladium-catalysed cross-coupling reactions of new *p*-phenyleneethynylene building blocks. Steady-state emission studies on the dyads **1-5** reveal a complicated behavior of the emission which is strongly medium dependent. In low polarity solvents the emission is characterized by a sharp high energy peak attributed to fluorescence from a locally excited (LE) state. In more polar environments the LE state is effectively quenched by transfer into an intra-molecular charge transfer (ICT) state. The medium dependence is also observed in the quantum yields (QYs) which are high in cyclohexane and low QYs in acetonitrile, thus also indicating charge transfer character. Low temperature emission spectra for **2-5** in dichloromethane and diethyl ether also reveal two distinct excited states, namely the LE state and the conventional ICT state, depending on solvent and temperature. Hybrid DFT calculations for **1-7** establish that the OPE bridge is involved in both frontier orbitals where the bridge character increases as

the bridge length increases. Computed TD-DFT data on **1-5** assign the emission maxima in cyclohexane as LE transitions. Each time-resolved emission measurement on **2-7** in cyclohexane and diethyl ether reveals a wavelength dependent bi-exponential decay of the emission with a fast component in the 5-61 ps range on blue detection and a slower ~1 ns phase, independent of detection wavelength. The fast component is attributed to LE fluorescence and this emission component is rate limited and quenched by transfer into an ICT state. The fast LE fluorescence component varies systematically with conjugation length for the series of D–B–A dyads **2-5**. An attenuation factor β of 0.15 $Å^{-1}$ was determined in accordance with an ICT superexchange mechanism.

Introduction.

Extensive studies have focused on covalently-linked donor–bridge–acceptor (D–B–A) compounds as "molecular wires" for investigating long distance ultrafast charge/excitation energy transfer.[1,2,3,4] Practical applications in optoelectronics and nanoscale science as well as fundamental knowledge of electron transfer (ET) processes relevant to both biological and chemical systems make this a vibrant topic.[5,6,7] The design of simplified molecular systems may allow the complex photochemical charge separation processes that occur in photosynthesis to be more easily modeled; this is of great interest for solar energy applications among others.[8] Rates of intramolecular charge transfer (ICT) in a D–B–A molecule depend on many factors including the nature of the donor, acceptor and bridge moieties, the distance between donor and acceptor, the orientation of the bridge and the electronic coupling between the donor, acceptor and bridge.[9,10,11]

ICT may occur by coherent tunneling (a superexchange mechanism) through the bridge, or by incoherent hopping via the bridge.[12] Tunneling occurs when donor and acceptor states mix with the bridge states, which are higher in energy than, and well separated from, the donor and acceptor. During the ICT process charge is not located on the bridge. The rate of superexchange ICT in these systems is dependent on an attenuation factor, denoted β, and displays exponential distance dependence and is thus given by equation (1);

$$k_{\mathrm{ICT}} = k_0 e^{-\beta(R-R_0)} \qquad (1)$$

where k_0 is the rate of ICT without a bridge segment, R_0 is the length of the D–A molecule without a bridge present and R is the length of the D-B-A molecule. The comparison of the β

value for D–B–A molecules having the same π-electron bridge but different D and A units demonstrates that β is a parameter of the entire system rather than being bridge specific.[2] For a molecular bridge to transport charge over long distances with good efficiency, the distance dependence of the ICT should be weak. This can occur when the energies of the bridge states are comparable to that of the donor, and the bridge may be oxidized or reduced directly with electron transfer occurring through a hopping mechanism. The distance dependence of this type of ICT mechanism is much weaker than for the superexchange mechanism and the hopping rate of ICT is inversely proportional to the distance between D and A moieties, i.e. $k_{\mathrm{ICT}} \propto \left(R - R_0\right)^{-1}$.

Oligo-*p*-phenyleneethynylene (OPE) derivatives are conjugated rigid rod-like molecules that can be functionalized internally and at the terminal positions.[13,14,15] These features make them attractive molecular bridges in D–B–A molecules. An OPE bridge (comprising three phenyl units) was shown to mediate efficient electron transfer between a donor zinc phthalocyanine and acceptors pyrrolidinoC_{60} or gold porphyrin with strong electronic coupling over a distance of >30 Å.[16,17] The excited-state dynamics of systems consisting of a zinc tetraphenylporphyrin and a free base tetraphenylporphyrin bridged by longer OPE units have been investigated using ultrafast spectroscopy.[18]

UV-Visible absorption studies on OPE wires terminated with dialkylamino donor and cyano, formyl or nitro acceptor groups showed a competition between the π–extension of the chromophores and a decrease of the ICT upon increasing the number of PE repeat units.[19] More extensive photophysical studies on series of extended-TTF–OPE–pyrrolidinoC_{60},[20,21] porphyrin–OPE–pyrrolidinoC_{60}[22] and 3,5-dimethyl-4-(9-anthracenyl)julolidine–OPE–naphthalene-bis(dicarboximide) systems[23] gave β values of 0.20, 0.11 and 0.23 Å^{-1}, respectively. Other examples include boron dipyrromethene (BODIPY)–OPE systems.[24,25] Electronic conduction through OPE wires anchored in metal–molecule–metal junctions has also been reported, with length dependent tunneling-to-hopping transitions observed.[26,27]

In the present investigation we focus on a new series of five D–B–A complexes **1**-**5** with OPEs of varying lengths (n = 0 – 4, respectively) as the bridges between diarylamino (D) and aryloxadiazole (A) moieties (Chart 1). The efficiency of ICT processes in these complexes is probed using absorption spectra, cyclic voltammetry, steady-state and time-resolved luminescence (or emission), supported by density functional theory (DFT)

calculations. The data obtained establish that efficient ICT in these systems occurs on a picosecond timescale essentially following a superexchange mechanism.

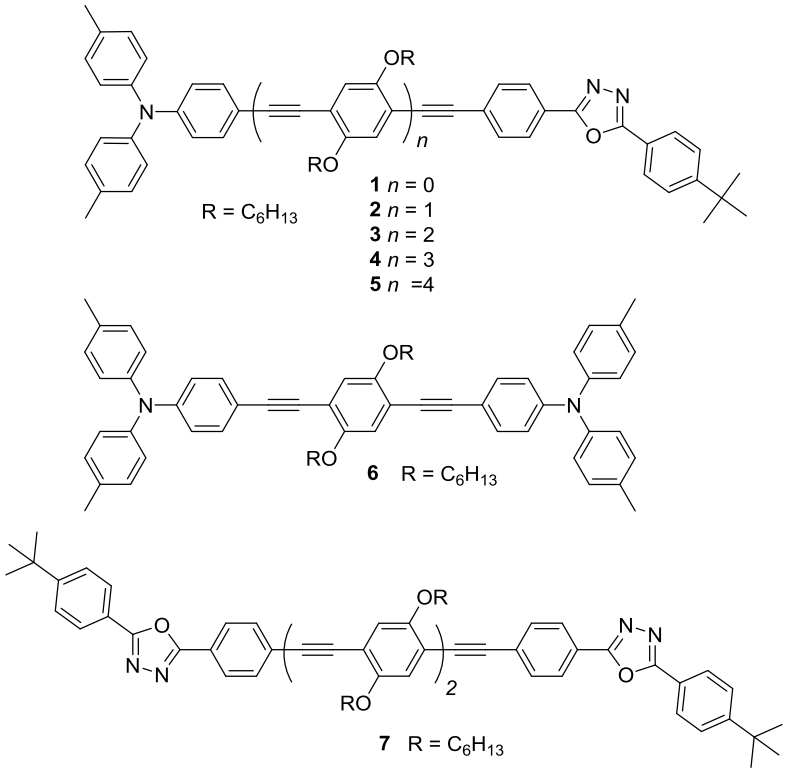

Chart 1. Structures of the molecules studied in this work. Systems **1** - **5** constitute D–A and D–B–A molecules while **6** is an A–B–A and **7** is a D–B-D molecule.

Results and Discussion.

Synthesis.

The structures of the D–B–A derivatives **1-5** and the symmetrical D–B–D and A–B–A reference compounds **6** and **7** studied in this work are shown in Chart 1. The synthetic strategies exploit iterative Pd-catalyzed Sonogashira cross-coupling reactions[28] of new *p*-phenyleneethynylene building blocks. The retrosynthetic disconnections of the molecules are based on: (i) commercial availability and ease of synthesis of the starting materials; (ii) high yielding reactions; (iii) intermediate species which could be easily purified, thereby facilitating the final step to the target D–B–A derivatives. Hexyloxy substituents are attached to the inner phenyl rings to give the molecules good solubility in organic solvents. As representatives of the series, the syntheses of **2** and **4** are shown in Scheme 1. The syntheses of the other analogues are presented in the Supporting Information along with schemes S1-S6. The target molecules were characterized by ^{1}H and ^{13}C NMR spectroscopy and mass

spectrometry which confirmed their expected structures and established their high level of purity.

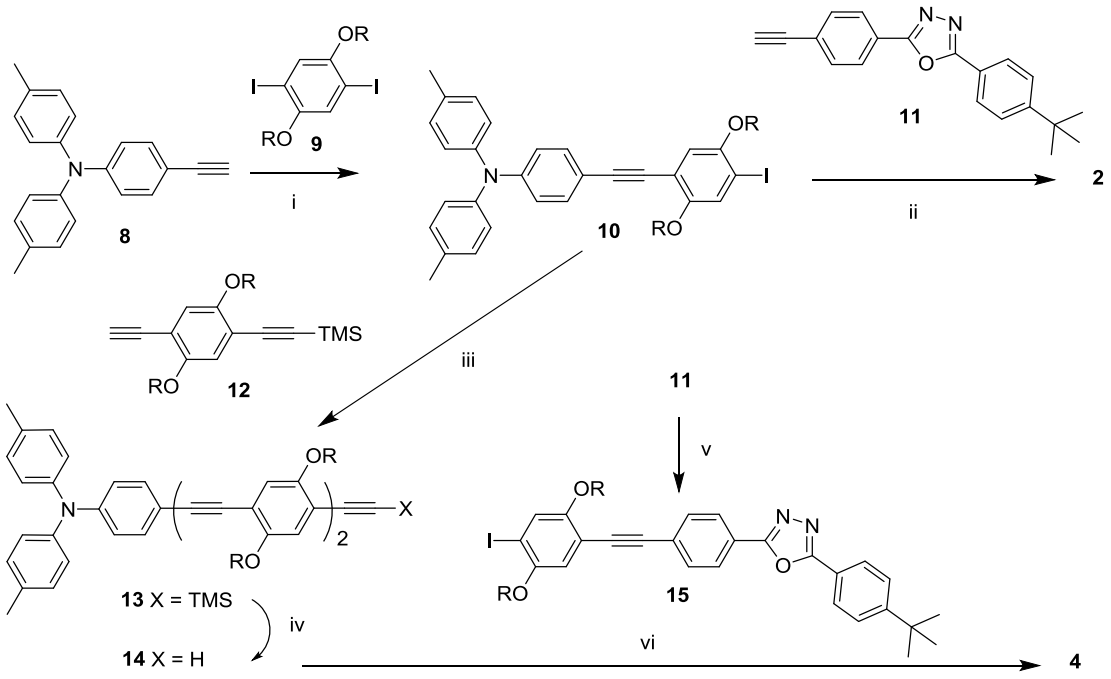

Scheme 1. Syntheses of D–B–A derivatives **2** and **4**.

Reagents and conditions: i) $[Pd(PPh_3)_4]$, CuI, Et_3N, reflux, 15 h, 53%; ii) $[PdCl_2(PPh_3)_2]$, CuI, Et_3N, 50 ^oC, 13 h, 86%; iii) $[Pd(PPh_3)_4]$, CuI, Et_3N, THF, reflux, 15 h, 87%; iv) K_2CO_3, MeOH, THF, 20 ^oC, 2 h, 100%; v) **9**, $[Pd(PPh_3)_4]$, CuI, Et_3N, THF, reflux, 15 h, 58%; vi) $[Pd(PPh_3)_4]$, CuI, Et_3N, THF, reflux, 15 h, 22%.

Solution electrochemistry.

The solution redox properties of **1-7** have been studied by cyclic voltammetry (CV) in acetonitrile and data are collated in Table 1. The oxidation potential of 0.46 V for **1**, assigned to the one-electron oxidation of the triarylamine unit, decreases to 0.40-0.42 V for the longer molecules **2-5** (Figure 1).[29,30] The symmetrical D–B–D compound **6** contains two oxidation waves only 120 mV apart, corresponding to sequential oxidations at the two (electronically interacting) triarylamine units.[31] Additional oxidation waves ascribed to the bridge unit are also observed at higher potentials (0.65-0.88 V) which shift cathodically from **2** to **5**. This shows that higher oxidation states are stabilized by the longer, more delocalised bridges.

Similar behavior was reported for an extended-TTF–OPE–pyrrolidinoC_{60} series.[20] Irreversible reduction waves were observed between -2.23 and -2.45 V for compounds containing the oxadiazole group.

Table 1. Electrochemical data for **1-7** in dry dichloromethane. All values in volts (V) with ferrocene/ferrocenium couple as internal reference at 0.00 V.

Compound	$E^{1/2}_{ox}$ [a]	$E^{1/2}_{ox}$ [b]	$E^{1/2}_{ox}$ [c]	E_{ox} [d]	E_{red} [e]	HLG [f]
1	0.46 [g]			1.00	-2.45	2.85
2	0.40 [g]	0.88 [h]		1.22	-2.37	2.71
3	0.40 [g]	0.79 [h]		1.12	-2.32	2.66
4	0.41 [g]	0.67 [h]		1.09	-2.32	2.67
5	0.42 [g]	0.65 [h]		0.82	-2.31	2.67
6	0.37 [g]	0.45 [g]	0.92 [h]	1.12	–	–
7	0.80 [h]			1.46	-2.23	2.97

a) Half wave potential for first reversible oxidation wave.
b) Second reversible oxidation wave.
c) Third reversible oxidation wave.
d) Anodic potential for first irreversible oxidation wave.
e) Cathodic potential for first irreversible reduction wave.
f) HOMO-LUMO energy gap based on cathodic wave potentials between first oxidation and reduction waves.
g) Oxidation at the triarylamine group.
h) Oxidation at the OPE bridge.

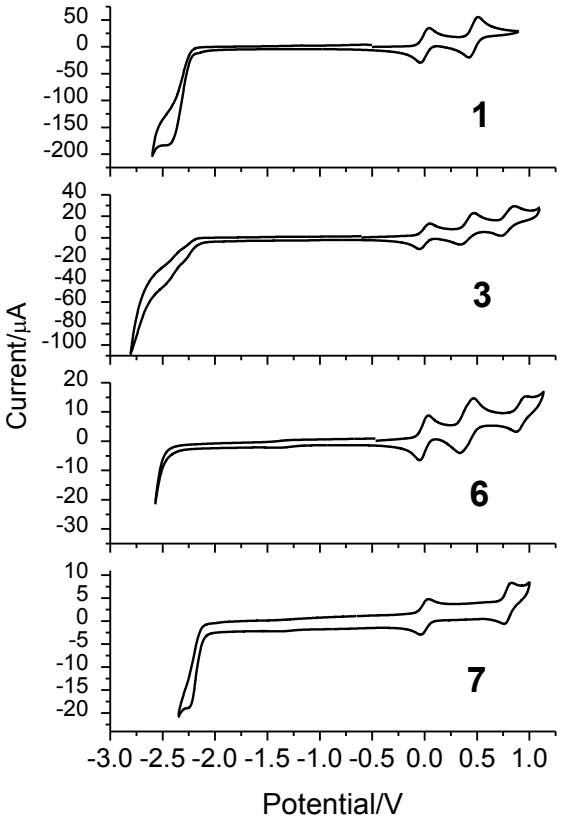

Figure 1. Cyclic voltammograms for **1**, **3**, **6** and **7** in dry dichloromethane with internal ferrocene/ferrocenium (FcH^+/FcH) couples at 0.0 V.

Steady state optical spectroscopy.

The normalized absorbance spectra for compounds **1-5** in cyclohexane show a gradual red shift with increasing length of the OPE bridge (Figure 2 and Table 2). This trend points to an increase in conjugation which in turn implies mixing between the electronic states of donor, bridge (OPE) and acceptor components. The absorption spectra are similar in polar acetonitrile and non-polar cyclohexane. (See Table 2 and Figure S1 for compound **2**). The longer molecules **4** and **5** contain much higher extinction coefficients than **1**-**3** suggesting that the long OPE bridges contribute strongly to these transitions.

In order to obtain a clearer picture of the intramolecular electronic overlap, and also to understand the impact of the solvent polarity, the two symmetric systems **6** (D–B–D) and **7** (A–B–A) were studied. Compound **6** has one OPE unit in the bridge and it is therefore compared with the D–B–A molecule **2**. The absorption data of **6** and **2** are very similar. Likewise, **7** and **3**, both with two bridging OPE units, reveal no notable difference in their spectral data (Table 2).

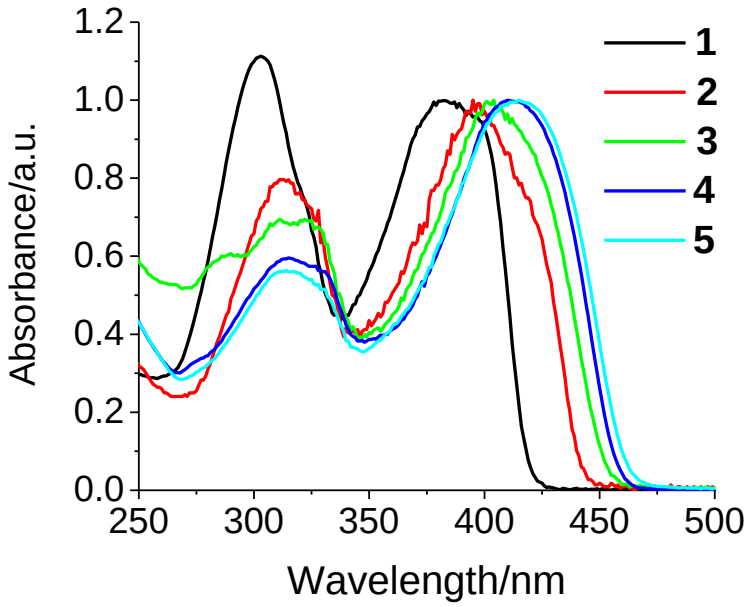

Figure 2. Absorbance spectra of **1**-**5** in cyclohexane where the intensities of the low-energy maxima are normalized to 1.0. See Table 2 and text for details.

In sharp contrast to the absorption spectra, the emission spectra of the D–A system **1** and the systems with bridging OPE units (D–B–A) **2** - **3** show a strong dependence on the dielectric medium (Table S1 and Figures 3, S2 and S3). The emission from longer D–B–A systems, **4** and **5**, and the symmetrical system **7** are not as strongly affected by the solvent polarity (Figures 3, S4 and S6). In non-polar solvents with a small Lippert-Mataga solvent density parameter Δf, ($\Delta f = \frac{\varepsilon_r - 1}{2\varepsilon_r + 1} - \frac{n_D^2 - 1}{2n_D^2 + 1}$, where ε_r is the relative permittivity and n_D is the refractive index), the emission from all compounds **1**-**7** is characterized by an intense sharp higher energy peak followed by a lower energy band shoulder, with a relatively small Stokes shift (1890-2650 cm^{-1} in cyclohexane, Table 1). The high energy peak is accordingly attributed to $S_0 \leftarrow S_1$ fluorescence from a locally excited (LE) state (*vide infra*) while the low energy broad shoulder could have charge transfer character, although some underlying vibronic contribution cannot be completely ruled out. This LE fluorescence behaviour is retained for **4** and **5** as the PL maxima values change little with more polar solvents. For **1** (D–A) and the shorter D–B–A complexes (e.g. **2** and **3**) the high energy peak disappears even for a modest increase in solvent polarity, while at the same time the broad low energy band increases in intensity and redshifts further with increased solvent polarity. This therefore suggests that the LE fluorescence is effectively quenched in **1, 2** and **3** in polar solvents,

leading to some decrease in the emission quantum yield (QY), compared to data in cyclohexane (Table 2). The broad low energy profile observed most clearly for **1, 2** and **3** in more polar media is therefore attributed to the formation of an ICT state due to its strong medium dependence.

For the two symmetric systems **6** and **7** ICT is not a possible excited state process and the consequence is therefore that the emission must be due to $S_0 \leftarrow S_1$ fluorescence. The fluorescence behaviour for **6** with a Stokes shift of 4320 cm^{-1} in acetonitrile suggests a substantial degree of solvatochromism (Figure S5). Previously a symmetric D–B–D amine-OPE-amine system like **6**, namely 1,4-$[(C_6H_{13})_2NC_6H_4CC]_2C_6H_4$ was reported to possess significant solvatochromism despite having an excited state with assumed overall zero dipole moment.[32] For **7** on the other hand, there is very little impact on the fluorescence with different medium polarity (Figure S6) both with respect to spectral progression and QY. This supports the notion that the significantly red-shifted emission in polar media for the shorter compounds **1**–**3** with Stokes shifts of 6970-8680 cm^{-1} can be ascribed to ICT states.[33,34,35]

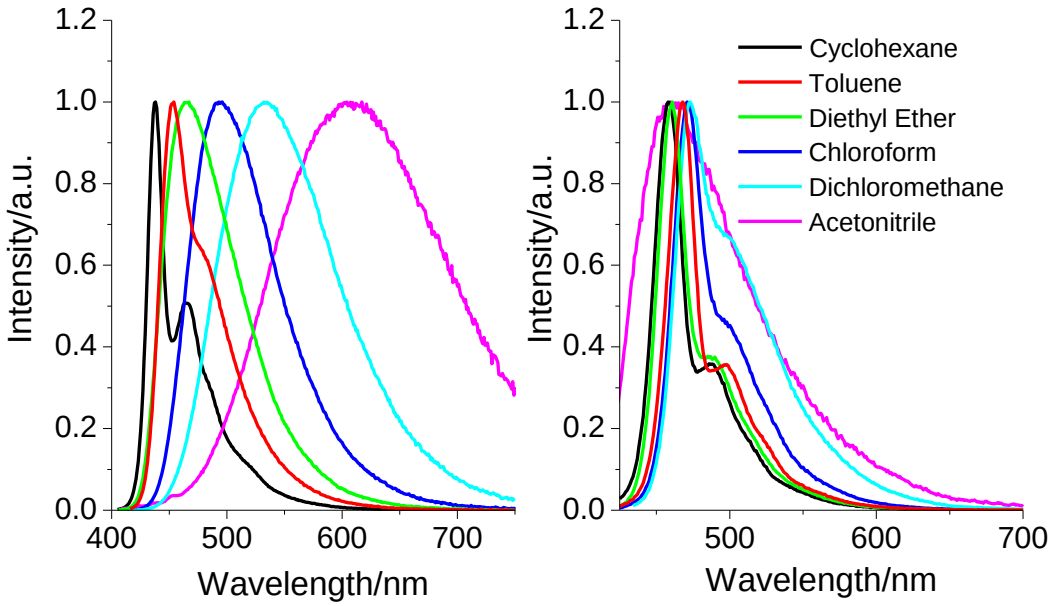

Figure 3. Normalized emission spectra of **2** (left) and **5** (right) for excitation at 385 nm in different solvents. See Tables 2 and S1 for data and text for details.

Interestingly, QYs of **1-7** in cyclohexane are high (0.89-0.94) and are independent of the chain length, apart from a lower QY of 0.71 for **5**. However, in polar acetonitrile the QYs of the D–B–A molecules **1–4** are considerably reduced to 0.15-0.21, whereas for the two symmetric analogues **6** and **7** the QYs remain high (0.82 and 0.96) while compound **5** is

lower (0.37). The decrease in the QYs for **1**-**4** resembles the decrease of QY from 0.94 to 0.10 on changing from cyclohexane to dichloromethane in a reported[36] D–π–A OPE system with dialkylamine as the donor group, 6-methylpyran-2-one as the acceptor group and –*para*-$C_6H_4CCC_6H_4CC$- as the OPE bridge. This molecule has a highly polar excited state with ICT properties. Such ICT excited states are also present in **1**-**4** based on their QY data.

It is also interesting to note differences in the photophysics of the series **2**–**4** studied in this work, and the related D–B–A dyads with electron-donor moieties (D=tetrathiafulvalene (TTF), bithiophene, 9-(4,5-dimethyl-1,3-dithiol-2-ylidene)fluorene and triphenylamine) connected to electron-accepting 2,5-diphenyl-1,3,4-oxadiazole (OXD) units.[30] Those latter systems had a different bridge segment without the hexyloxy substituents on the phenyl rings. In that case, the electronic coupling was strongly affected by bridge length (conjugation) leading to a dramatic decrease of the QY according to the energy gap law.[30]

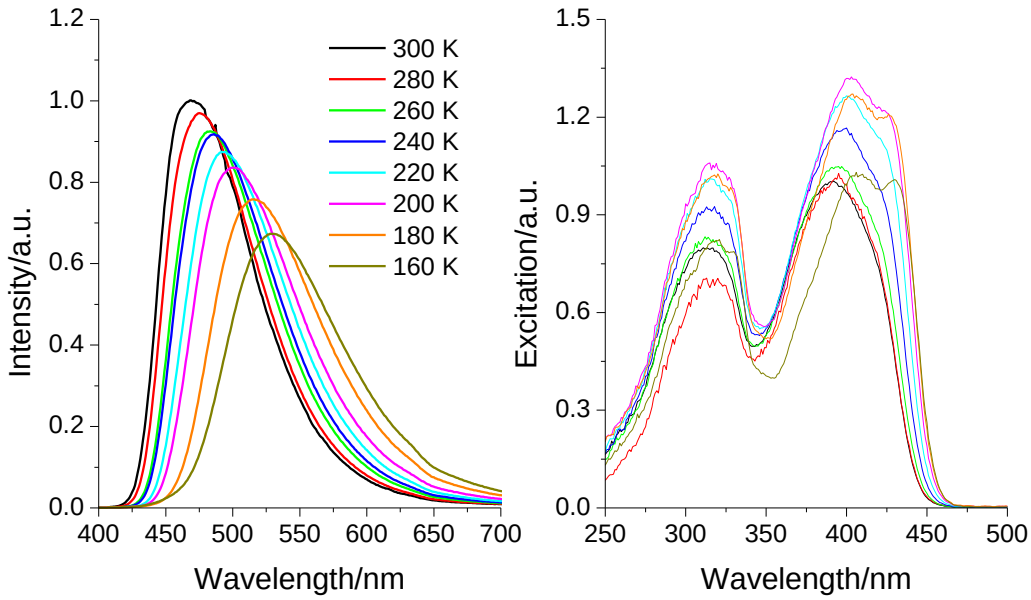

Figure 4. Emission (left) and excitation spectra (right) of **2** in diethyl ether at various temperatures. The emission maximum at 300 K is normalized to 1.0 and emission spectra at lower temperatures are scaled accordingly. The low energy profile in the excitation spectrum at 300 K is also normalized to 1.0 and excitation spectra at lower temperatures are scaled accordingly.

Low temperature optical spectroscopy was performed on compounds **2** - **7** in polar dichloromethane and the relatively non-polar diethyl ether: these solvents were chosen as they have the lowest melting points of the media used here. Figure 4 shows the emission and

excitation spectra for **2** in diethyl ether from ambient temperatures to just above the freezing point of the solvent. The lack of vibronic structure in the emission band suggests that this is from the ICT state. There is a gradual red shift of the emission and a small decrease in the intensity as the temperature is lowered. The excitation spectra of **2** in diethyl ether also display a gradual increased red shift; furthermore, the low energy absorption band is split into two distinctive profiles below 200 K. The increase in the red shift and in the structure of the low energy band on lowering the temperature suggests a higher population of planar conformers is present at lower temperatures. These data point to increasing stabilisation of the assumed planar ICT state at low temperatures, even in a non-polar solvent. The low temperature spectra of **3** in diethyl ether show that the ICT emission is induced as the temperature is lowered (Figure S7) like **2**.

Table 2. Photophysical data for compounds **1-7** in cyclohexane (CyH) and acetonitrile (MeCN).

Compound	λ_{abs} (nm) CyH	ε (cm^{-1} mol^{-1} dm^3)[a] CyH	λ_{em} (nm)[b] CyH	Stokes Shift (cm^{-1})[c] CyH	PLQY CyH[d]	λ_{abs} (nm) MeCN	λ_{em} (nm)[b] MeCN	Stokes Shift (cm^{-1})[c] MeCN	PLQY MeCN[e]
1	303, 384	46600, 41900	417, 437	2060	0.92	300, 381	555	8230	0.19
2	313, 396	12400, 15300	438, 465	2420	0.90	314, 398	608	8680	0.21
3	322, 402	20800, 29100	450, 478	2650	0.90	324, 408	573	6970	0.15
4	318, 412	98100, 165000	456, 485	2340	0.94	320, 417	485	3360	0.16
5	314, 415	76700, 138000	458, 488	2260	0.71	322, 411	462	2690	0.37
6	300, 396	35600, 65600	428, 451, (473)[f]	1890	0.94	297, 401	485	4320	0.96
7	329, 399	33900, 44200	445, 472, (494)[f]	2590	0.89	328, 405	454, (478)[f]	2665	0.82

a) Extinction coefficient.
b) Excitation at lowest energy λ_{abs} of the compound in specified solvent.
c) Difference in energy between lowest energy maximum λ_{abs} and highest energy maximum λ_{em}.
d) PLQYs measured in cyclohexane solution with excitation at lowest energy λ_{abs} of compound in cyclohexane; estimated error of ±0.05.
e) PLQYs measured in acetonitrile solution with excitation at lowest energy λ_{abs} of the compound in acetonitrile; estimated error of ±0.05.
f) Shoulder.

For **4** and **5** in diethyl ether, the emission spectra display vibronic structure and only minor changes as the temperature is lowered, thus indicating that the emission is primarily fluorescence from the LE state (Figures S8 and S9). This clearly demonstrates sensitivity of bridge length with relation to the formation of the ICT state. In parallel, the excitation spectra of **3**, **4** and **5** in diethyl ether do now show the same complicated behaviour as is observed for **2** (Figure 4) as these D–B–A complexes thus exhibit a more homogenous low energy band in the emission (Figures S7-S9). While the emission and excitation spectra for **2** in dichloromethane (Figure S12) resemble those of **2** in diethyl ether, the spectra for **3**, **4** and **5** in dichloromethane on varying the temperatures are dramatic (Figures S13, S14 and 5, respectively). The emission spectra for **3** and **4** show broad bands indicating ICT and the intensities rapidly decrease on lowering the temperature. However, for **5** in dichloromethane the emission spectrum at ambient temperature shows clearly a high energy peak ($S_0 \leftarrow S_1$ fluorescence from the LE state) which is reduced in intensity as the temperature is lowered and a broad unstructured red-shifted profile (ICT state) dominates the emission.

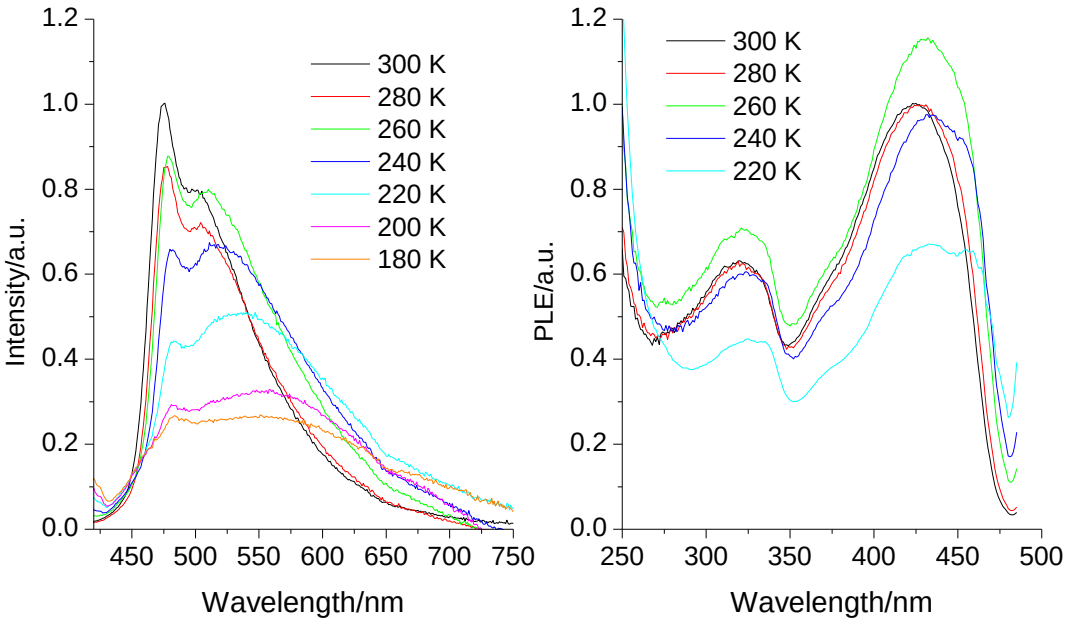

Figure 5. Emission (left) and excitation spectra (right) of **5** in diethyl ether at various temperatures. The emission maxima at 300 K are normalized to 1.0 and emission spectra at lower temperatures are scaled accordingly. The low energy profile in the excitation spectrum at 300 K is also normalized to 1.0 and excitation spectra at lower temperatures are scaled accordingly.

The low temperature data also show variations in the emission intensity and although corrections for any temperature variations in absorption cross-section at the excitation wavelength have not been performed, the data show a clear decrease of the intensity, therefore by implication also a decrease for the QY. The most dramatic decreases are observed for **3**, **4** and **5** in dichloromethane, while there is only a small change in intensities for the same compounds in diethyl ether. Analogue **2** on the other hand, does not display such intensity variation with dielectric media. The intensity variations are in line with the reduction in PLQY observed when the D–B–A complexes are in more polar media. This induces a conversion of the excited state into a less emissive ICT state which can also be achieved by lowering the temperature as discussed here.

Low temperature emission and excitation spectra were also obtained for the symmetric systems **6** and **7** in diethyl ether (Figures S10 and S11) and dichloromethane (Figures S15 and S16). Compared to the D–B–A complexes with similar length OPE bridge (**1** and **2**) it is evident that there is not the same dependence on the emission with temperature. Variations are modest and this in turn suggests that the emission in both compounds is $S_0 \leftarrow S_1$ fluorescence. It is also interesting to note the similarities between the emission spectra of **4**, **5** and **7** in diethyl ether. This indicates that the source of the emission is of similar character in these systems.

The ambient temperature emission spectra obtained for **1-5** in solvents of different polarities, in combination with the low temperature PL spectra, provide a clearer picture of the external and internal factors that influence the nature of the excited states in these systems. The polarity of the solvents is the most important factor for the conversion of the excited state into an ICT state. However, by extending the OPE bridge length between the D and A moieties an equilibrium between the LE state and the ICT state is established, even in more polar media. By subsequently lowering the temperature, the equilibrium will be shifted towards the ICT state which accordingly is the main source of the emission under these conditions.

Molecular Orbital Computations.

Ground state (S_0) geometry optimizations were carried out on molecules **1-7** at the B3LYP/6-31G* level without symmetry constraints where methyl groups were used instead of hexyl groups in **2-7** to reduce computational efforts. All the optimized geometries are denoted by the suffix **a**, i.e. **1a-7a**.

Electronic structure calculations on **1a-7a** show that the HOMOs are on the amine and bridge with considerable π-conjugation, whereas the LUMOs also contain π-conjugation within the oxadiazole and bridge. The amine and oxadiazole contributions to these frontier orbitals decrease on going from **1a** to **5a** (Tables 3 and S2, Figures 6 and 7). The bridge contributions increase in both frontier orbitals as the D–B–A molecule is lengthened. The increased donor and acceptor contributions to the HOMO and LUMO reflect the experimentally observed increased solvatochromic shifts on emission, indicating that the emissions are charge transfer in character, unlike the observed small solvatochromic shifts in the absorption spectra. The bridge contribution to the frontier orbitals also increases from the symmetrical D-B-D molecule **6a** containing one OPE link to the longer A-B-A molecule **7a** with two OPE units.(Figure S17 and Table S2)

Table 3. Comparison of donor (D = Tol_2N) contribution in HOMO and acceptor (A = $tBuC_6H_4C_2N_2O$) contribution in LUMO vs observed solvatochromic shifts for **1a-7a**.

	D contribution in HOMO (calc, %)	A contribution in LUMO (calc, %)	Bridge Length R-R_0 (Å)[a]	Absorption solvatochromic shift (cm^{-1})[b]	Emission solvatochromic shift (cm^{-1})[c]
1a	54	35	0.0	205	5960
2a	40	22	6.9	-130	6380
3a	29	17	13.7	-370	4770
4a	22	13	20.5	-290	1310
5a	17	12	27.3	240	190
6a	36[d]	-	6.9	-315	2750
7a	-	16[d]	13.7	-372	450

a) Bridge length (R-R_0) where length of R_0 is length of **1** and R is length of corresponding molecule from optimized S_0 geometries.
b) Energy difference between the observed lowest energy maxima λ_{abs} in cyclohexane and in acetonitrile.
c) Energy difference between the observed highest energy maxima λ_{em} in cyclohexane and in acetonitrile.
d) Sum from both groups.

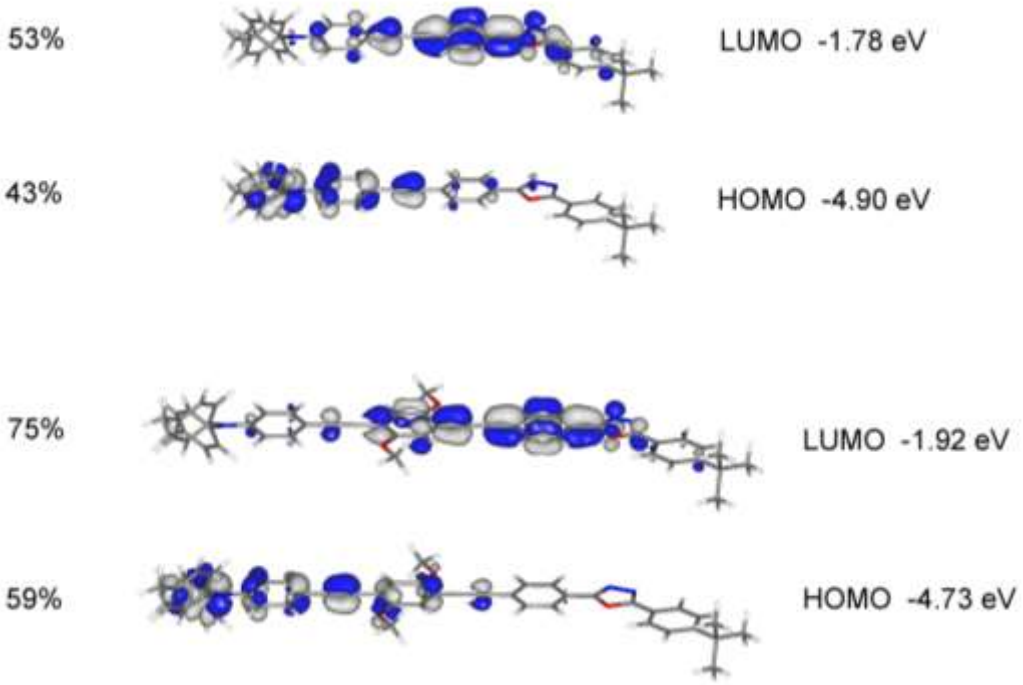

Figure 6. Frontier orbitals for **1a** (upper pair) and **2a** (lower pair). Contours drawn at +/-0.04 $(e/bohr^3)^{1/2}$. The values in % correspond to bridge character in the orbital.

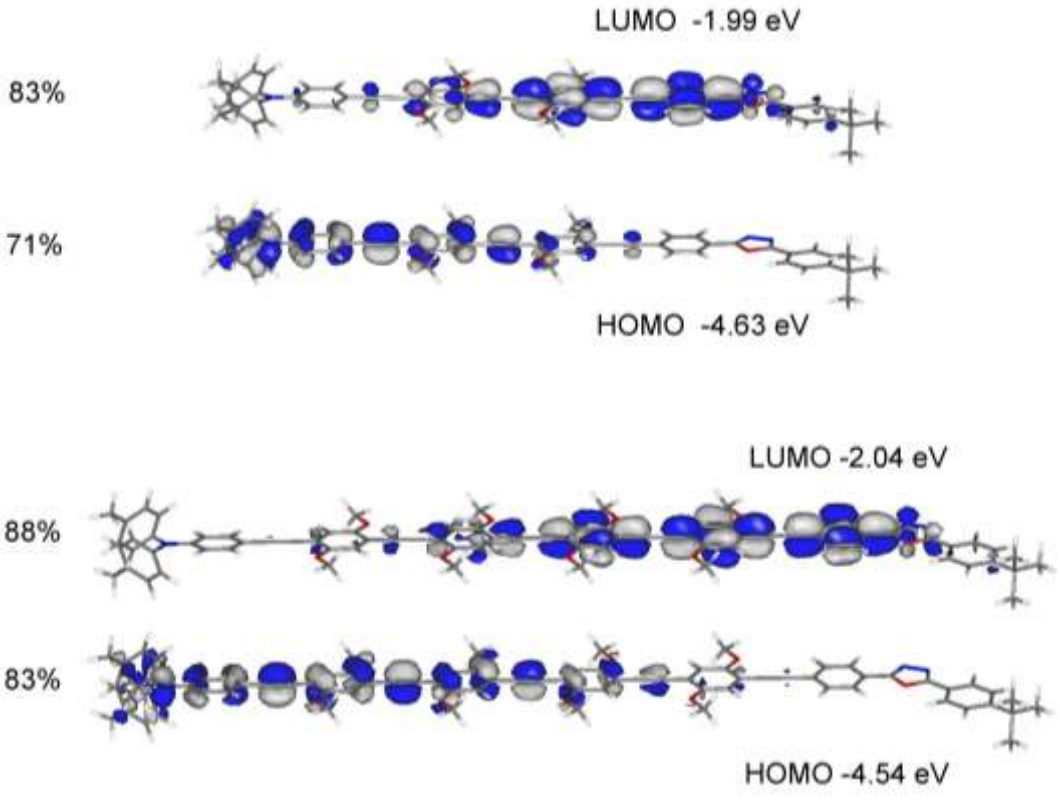

Figure 7. Frontier orbitals and energies for **3a** (upper pair) and **5a** (lower pair). The bridge coefficients for LUMO and HOMO in **4a** are 87% and 78% respectively.

Figure S18 summarises the energy levels of the HOMO and LUMO along with selected orbitals that are close to the LUMO or HOMO in energies. The agreement between the trend in HOMO energies for **1a-7a** and the trend in the oxidation potentials corresponding to triarylamine oxidations (Table 1) for **1-7** is good. The oxidation waves observed at ca 0.65-0.82 V in the CV data for **2-5** correspond to bridge oxidations as their HOMO+1 levels are located at the bridges. Their energies increase on going in length from **2** to **5** in accord with the trend of decreasing potentials observed from **2** (0.82 V) to **5** (0.65 V).

TD-DFT computations were carried out on **1a-7a** at CAM-B3LYP/6-31G* to predict the absorption maxima and the nature of the transition bands. The hybrid functional CAM-B3LYP is used to compute charge transfer transitions as it has the necessary physics to model charge contributions more correctly than the widely used B3LYP functional.[37] TD-DFT data are summarised in Table 4 along with observed absorption data. The trend of the calculated absorption maxima is in broad agreement with observed maxima. The lowest energy bands observed for the D-B-A molecules **2a**-**5a** are assigned as π(amine-bridge)-π*(bridge-oxadiazole) transitions with sequentially increased bridge character in both orbitals on going from **2a** to **5a**. OPE molecules, of similar length to **5a**, such as 2,5-$(MeO)_2C_6H_3[CCC_6H_2(OMe)_2]_3C_6H_4CN$-4, have essentially LE character in both absorption and emission.[38] The higher energy bands observed in **2a**-**5a** are assigned as π(bridge)-π*(bridge) dominated LE transitions.

Table 4. TD-DFT data for **1a-7a** and comparison with observed absorption maxima for **1-7** in cyclohexane (D = diarylamine group, B = bridging unit, A = aryloxadiazole group).

	Calc. Abs. (nm)	Oscillator strength (*f*)	Major MO Contributions	Transition Type	Obs. Abs. (nm)
1a	285	0.25	HOMO-1 → LUMO	π (BA) → π*(BA)	303
	354	2.20	HOMO → LUMO	π(DB) → π*(BA)	384
2a	296	0.38	HOMO-2 → LUMO	π (BA) → π*(BA)	313
	389	2.91	HOMO → LUMO	π (DB) → π*(BA)	396
3a	305	0.43	HOMO-2 → LUMO	π (B) → π*(BA)	322
	410	3.71	HOMO → LUMO	π (DB) → π*(BA)	402
4a	323	0.51	HOMO-1 → LUMO+1	π (DB) → π*(B)	318
	425	4.51	HOMO > LUMO	π (DB) → π*(br/ox)	412
5a	339	0.60	HOMO → LUMO +1	π (DB) → π*(B)	314
	434	5.37	HOMO → LUMO	π (DB) →> π*(BA)	415
6a	295	0.17	HOMO-2 → LUMO	π (B) → π*(B)	300
	383	2.82	HOMO → LUMO	π (DB) → π*(B)	396
7a	301	1.15	HOMO-2 → LUMO	π (BA) → π*(BA)	329
	410	3.81	HOMO → LUMO	π (B) → π*(BA)	399

The computed absorption maxima for **2a** and **6a** with similar molecular lengths agree with those observed experimentally for **2** and **6** in non-polar media. Such similarities also apply to the longer molecules, **3a**, **7a**, **3** and **7**. These pairs of molecules may be regarded as simple OPEs where the D and A groups have little influence on the strong absorption bands arising from LE transitions. The parent OPE molecule, $PhCCC_6H_2(OC_6H_{13})_2CCPh$, where the donor and acceptor groups are replaced by hydrogen groups in **2a**, has absorption maxima at 307 and 367 nm in methylcyclohexane assigned by TD-DFT computations elsewhere as HOMO-1 → LUMO and HOMO → LUMO LE transitions, respectively.[39]

Excited state geometries on model geometries **1b-7b** were optimized using TD-DFT computations at CAM-B3LYP/6-31G*. These model geometries denoted with suffix **b** contain no alkyl groups at the end groups to reduce computational efforts. All these optimized excited state geometries **1b-7b** have all the OPE phenylene and oxadiazole rings in plane and their predicted emission maxima are in broad agreement with observed emission maxima in cyclohexane as viewed in Table 5. Such agreements between observed and computed emission data have been found in a related D-π-A OPE derivative study.[40] The calculated Stokes shifts of 1720-2670 cm^{-1} are in the same region as the observed Stokes shifts of 1890-2650 cm^{-1} in cyclohexane (Table 2).

Table 5. TD-DFT data for optimized excited state geometries **1b-7b** and comparison with observed emission maxima for **1-7** in cyclohexane (D = diarylamine group, B = bridging unit, A = aryloxadiazole group).

	Calc. Em. (nm)	Oscillator strength (*f*)	$S_0 \leftarrow S_1$ Transition Type	Calc. Stokes shift (cm^{-1})	Obs. Em. (nm)
1b	391	2.17	π(DB) ← π*(BA)	2670	417
2b	429	2.84	π (DB) ← π*(BA)	2400	438
3b	451	3.56	π (DB) ← π*(BA)	2220	450
4b	463	4.28	π (DB) ← π*(BA)	1930	456
5b	469	5.01	π (DB) ← π*(BA)	1720	458
6b	422	2.78	π (DB) ← π*(B)	2610	428
7b	450	3.58	π (B) ← π*(BA)	2170	445

Time-resolved emission spectroscopy.

Time domain studies were performed at ambient temperature using the well-known time-correlated single photon counting (TCSPC) technique. Pulsed excitations in the low energy absorption bands of the series of D–B–A compounds reveal a complicated picture of the excited state dynamics that is strongly influenced by the dielectric medium. It was not possible using our TCSPC system to record the time-resolved emission of **1** in any medium and determine the emission dynamics, details on this are given in the supporting information.

In cyclohexane with blue detection, the decay of the emission is dominated by a fast component in the 16–60 ps (Table S3 and Figures 8, Figures S19-S21) for the D–B–A compounds **2** – **5**. This decay phase is followed by a slower emission component in the 770–993 ps range. For more red detection of the emission this component can no longer be observed; instead a single exponential decay is observed in the 770–970 ps range and the rate of this decay decreases for the longer compounds. The yield (calculated from the lifetime amplitude product: $\tau_i \times A_i$) of this slower component is between 78 and 94% and shows a random variation across the series **2** – **5**.

For more polar solvents, i.e. diethyl ether and dichloromethane, there is dramatic impact on the emission decay as is evident in Figures 8, S19-21 and Table 6. For **2** in dichloromethane the decay is characterized by a single exponential component in the ~35 ns range. The repetition rate of the excitation pulses is 76 MHz which corresponds to ~13 ns pulse-to-pulse window. It is clearly seen that the emission signal has not yet decayed to zero intensity before the next pulse excites the sample again. A further complication is that the

formation of metastable states as a consequence of the repetition rate of the excitation pulses and the long excited state lifetime is not ruled out. Consequently, it is therefore possible to make only an estimate of the emission lifetime of **2** in dichloromethane. For the more conjugated systems **3** – **5** in polar solvents, the emission decay is faster and therefore contained within the pulse-to-pulse window and the decay of the emission can be fitted to a single exponential model.

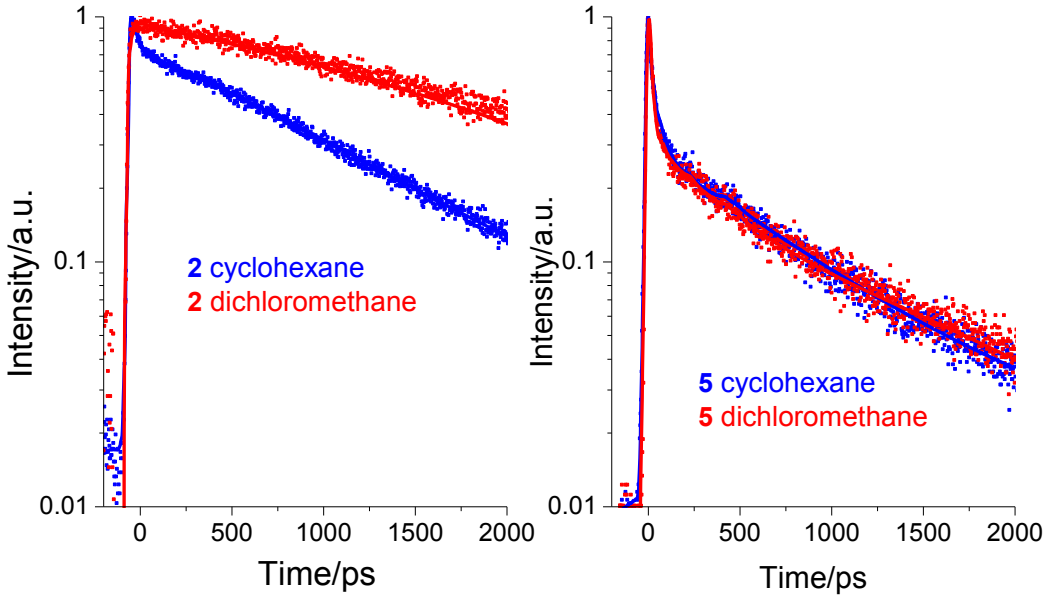

Figure 8. Emission decays recorded at the blue edge of the spectra of **2** (left) and **5** (right) in cyclohexane and dichloromethane: λ_{exc} 385 nm. See Table S3 for data and text for details.

For the series of D–B–A complexes we observe in polar media a very strong stabilisation of an ICT state, especially for the shorter bridge lengths (**2** and **3**). This conclusion is based on: i) the gradual increase in emission lifetime when the D–B–A complexes are dissolved in more polar media with a particularly dramatic increase observed for **2** in dichloromethane and ii) that the fast 10-20 ps range component is not observed for **2** and **3** in dichloromethane. The rate of the fast component increases when **2** and **3** are dissolved in diethyl ether as compared to cyclohexane. It is, therefore, highly likely that for **2** and **3** in dichloromethane it escapes detection due to the time-resolution of our TCSPC system, which further supports the conclusion of a fast and strong stabilisation of the ICT state in those D–B–A complexes under these conditions. However, for compounds **4** and **5** with longer bridges, even in polar media, it is apparent that the ICT state is not readily

formed. In these cases the emission has, instead, more of the character of $S_0 \leftarrow S_1$ fluorescence from an LE state.

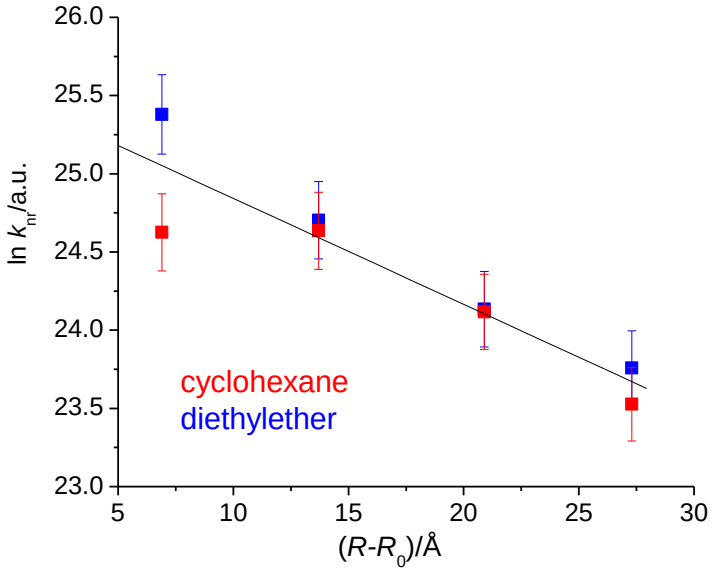

Figure 10. Data for the rate of ICT in cyclohexane and diethyl ether as a function of molecular length for compounds **2-5** and a fit of the data (solid line) using equation 1. The molecular length corresponds to the bridge length i.e. -[CC-$C_6H_2(OR)_2$]$_n$- and the bridge lengths used here are obtained from the calculated and optimized S_0 geometries as listed in Table 3. Rate constants have been obtained from the kinetics listed in Table 6. For the linear regression R^2 = 0.93. See text for details.

For the series of D–B–A complexes, the fast emission component observed only in the blue is therefore attributed to the dynamics of the LE $S_0 \leftarrow S_1$ fluorescence which in turn is quenched and limited by the planarisation of the D–B–A complexes and the subsequent transfer into/formation of the ICT state. The fact no such phase is observed in the time-domain experiments for the D–A compound **1** can be due to the rate of formation of the ICT state in that system, which is faster than the time-resolution of the TCSPC system used in this work. However, as previously commented it was very difficult to measure the emission decay in **1** (see Figure S19) and this may also have contributed. Hence, k_0 is equation 1 is in principle an experimentally accessible parameter from **1** but not measured for the reasons mentioned above.

Figure 10 shows a plot of the dynamics of the fast fluorescence component for **2-5** against wire length in two different solvents. In this analysis the ICT process is assumed to occur from D-to-A in the D–B–A molecules and the length variation therefore includes a correction term (R_0 in equation 1).[21,23,38] The experimental data can be readily fitted to equation 1 giving an attenuation factor of β = 0.15 Å^{-1}. This is intermediate between the

values of β = 0.11 Å^{-1} reported previously for porphyrin–OPE–pyrrolidinoC_{60} systems,[22] and β = 0.20 Å^{-1} for extended-TTF–OPE–pyrrolidinoC_{60}.[20,21] These relatively large values for OPE bridges indicate that the length of the bridge has a significant impact on the ICT process. For comparison, oligo-*p*-phenylenevinylene (OPV) bridges, albeit with different D and A moieties, can give much lower β values, indicative of more effective conjugation, e.g. *tetra*-phenylporphyrin (TPP) conjugates[41] TPP-OPV-pyrrolidinoC_{60} 0.03 Å^{-1}, and exTTF-OPV-pyrrolidinoC_{60} gives an exceptionally small β value of 0.01 Å^{-1}.[42]

The emission from the symmetric systems **6** and **7** also display a fast component in the blue detected in non-polar and polar media. The emissions must therefore have the character of $S_0 \leftarrow S_1$ fluorescence, irrespective of solvent polarity. However, **6** did show more medium dependency in the steady state emission which was attributed to solvatochromism, as previously mentioned. It is therefore possible that this could be reflected in the time domain emission as well. However, a more likely interpretation of the fast emission component in both systems is that this phase reflects structural relaxation or planarisation of their conformations. The dynamics of this process appears to be correlated with the molecular size as **6** is faster than **7** in both solvent media (Table 6).

Conclusions

The synthesis and optoelectronic properties are reported for an extended series of novel dyads **1**-**5** with OPE bridges and triarylamine donor and diaryloxadiazole acceptor end groups. These systems have high PLQYs in cyclohexane where the OPE bridges play a dominant role. In low polarity solvents the emission is characterized by a sharp high energy peak attributed to fluorescence from a locally excited (LE) state. In more polar environments the LE state is effectively quenched by transfer into an intra-molecular charge transfer (ICT) state. The ICT state also dominates at lower temperatures. An attenuation factor β of 0.15 Å^{-1} was determined for dyads **2-5** by time-resolved emission measurements in accordance with an ICT superexchange mechanism. This value compliments those reported in previous studies on OPE wires with very different D and A end groups. The experimental results are well supported by molecular orbital computations. Overall these data will assist in the future design of new multichromophore D-B-A systems with long-range photoinduced molecular wire properties of relevance to organic electronics.

Experimental Section

Details on syntheses and characterization of new compounds **1**-**7** are given in the Supporting Information.

Optical spectroscopy.

Linear absorption spectra were recorded on a UV-vis vision absorption spectrometer. Fluorescence and emission spectra were recorded on a Jobin-Yvon Horiba fluorolog tau3 instrument. In the fluorescence experiments spectroscopic grade solvents were used and the absorption maximum did not exceed 0.3. Quantum yields (QYs) were measured using the absolute method.[43]

Time-resolved emission was measured using the time-correlated single photon counting technique (TCSPC). A Verdi V8 green diode laser pumps a picosecond Mira 9000 Ti:Sapphire β mode-locked tuneable oscillator cavity. The wavelength of laser emission is in the near infrared (NIR) at 780 nm. The pulses are passed through a BBO crystal (type I) aligned on a micrometer support to generate the second harmonic at 390 nm. The mixed 780 nm/390 nm beam is then split at a layered dielectric mirror that reflects the NIR component onto a photodiode providing the stop pulse in the TCPSC system. The 390 nm component is subsequently focused onto the sample. The emission is collected through a filter to remove the laser scatter, and focused into a SpectraPro-2300i double subtractive monochromator (Acton Research Corporation) for emission wavelength selection and subsequently directed onto the TCSPC detector. The detector is a water-cooled 6 micron Hamamatsu E3809U-50 MCP photomultiplier tube for single photon detection directly attached to the double-monochromator assembly. The computer attached to the detector has a Becker & Hickl SPC-630 Time-Correlated Single-Photon Counting (TCSPC) card. The laser pulses measured by the system (incorporating the detector response characteristics) have a full width half maximum of 21-23 ps. The emission decays are fitted to a sum of exponentials (equation 2)

$$F(\lambda_{em},t)=\sum_i A_i(\lambda_{em})\cdot e^{-k_i\cdot t} \qquad (2)$$

using a deconvolution/convolution procedure with the optical/electronic response function of the detection system. The quality of the fits was judged based on the χ^2 parameter and visual inspection of the weighted residuals.

Solution electrochemistry.

Electrochemical measurements (Autolab PG-STAT 30) were carried out using dry dichloromethane solutions of ca. 10^{-4} M analyte containing 0.1 M NBu_4PF_6 electrolyte in a standard three-electrode cell using platinum (1 mm diameter disc) working electrode with platinum wires as counter and reference electrodes. Potentials are reported using a ferrocenium/ferrocene couple (FcH^+/FcH = 0.0 V) as an internal reference.

Acknowledgement. We thank EPSRC for funding.

References.

[1] D. K. James, J. M. Tour, *Top. Curr. Chem.* **2005**, *257*, 33-62.

[2] E. A. Weiss, M. R. Wasielewski, M. A. Ratner, *Top. Curr. Chem.* **2005**, *257*, 103-133.

[3] D. M. Adams, L. Brus, C. E. D. Chidsey, S. Greager, C. Creutz, C. R. Kagan, P. V. Kamat, M. Lieberman, S. Lindsay, R. A. Marcus, R. M. Metzger, M. E. Michel-Beyerle, J. R. Miller, M. D. Newton, D. R. Rolison, O. Sankey, K. S. Schanze, J. Yardley, X. Zhu, *J. Phys. Chem. B* **2003**, *107*, 6668–6697.

[4] (a) M. Gilbert, B. Albinsson, *Chem. Soc. Rev.* **2014**, DOI:10.1039/c4cs00221k. (b) D. M. Guldi, B. M. Illescas, C. M. Atienza, M. Wielopolski, N. Martin, *Chem. Soc. Rev.* **2009**, *38*, 1587–1597.

[5] F. Scandola, C. Chiorboli, M. T. Indelli, M. A. Rampi, in "*Electron transfer in chemistry"* (Ed.: V. Balzani), Wiley, Weinheim, **2001**, Vol. III, chapter 2.1.

[6] Special Issue on Organics and Optoelectronics, *Chem. Rev.* **2007**, *107*, 923-1386.

[7] A. C. Benniston, *Chem. Soc. Rev*. **2004**, *33*, 573–578.

[8] M. R. Wasielewski, *J. Org. Chem.* **2006**, *71*, 5051-5066.

[9] B. Albinsson, M. P. Eng, K. Pettersson, M. U. Winters, *Phys. Chem. Chem. Phys.* **2007**, *9*, 5847-5864.

[10] M. P. Eng, B. Albinsson, *Chem. Phys*. **2009**, *357*, 132-139.

[11] O. S. Wenger, *Acc. Chem. Res*. **2011**, *44*, 25−35.

[12] G. Zhou, M. Baumgarten, K. Müllen, *J. Am. Chem. Soc.* **2007**, *129*, 12211-12221.

[13] U. H. F. Bunz, *Chem. Rev*. **2000**, *100*, 1605-1644.

[14] N. M. Jenny, M. Mayor, T. R. Eaton, *Eur. J. Org. Chem*. **2011**, 4965-4983.

[15] K. Jennum, M. Vestergaard, A. H. Pedersen, J. Fock, J. Jensen, M. Santella, J. J. Led, K. Kilså, T. Bjørnholm, M. B. Nielsen, *Synthesis* **2011**, 539-548.

[16] E. Goransson, J. Boixel, J. Fortage, D. Jacquemin, H-C. Becker, E. Blart, L. Hammarstrom, F. Odobel, *Inorg. Chem.* **2012**, *51*, 11500−11512.

[17] F. Odobel, J. Fortage, *C. R. Chimie* **2009**, *12*, 437-449.

[18] G. Duvanel, J. Grilj, E. Vauthey, *J. Phys. Chem. A* **2013**, *117*, 918−928.

[19] H. Meier, B. Mühling, H. Kolshorn, *Eur. J. Org. Chem*. **2004**, 1033-1042.

[20] C. Atienza, N. Martin, M. Wielopolski, N. Howarth, T. Clark, D. M. Guldi, *Chem. Commun*. **2006**, *30*, 3202-3204.

[21] M. Wielopolski, C. Atienza, T. Clark, D. M. Guldi, N. Martin, *Chem. Eur. J.* **2008,** *14*, 6379-6390.

[22] A. Lembo, P. Tagliatesta, D. M. Guldi, M. Wielopolski, N. Nuccetelli, *J. Phys. Chem. A* **2009**, *113*, 1779-1793.

[23] A. M. Scott, A. B. Ricks, M. T. Colvin, M. R. Wasielewski, *Angew. Chem. Int. Ed*. **2010**, *49*, 2904-2908.

[24] A. Harriman, L. J. Mallon, K. J. Elliot, A. Haefele, G. Ullrich, R. Ziessel, *J. Am. Chem. Soc*. **2009**, *131*, 13375-13386.

[25] S. Yin, V. Leen, C. Jackers, D. Beljonne, B. V. Averbeke, M. V. der Auweraer, N. Boens, W. Dehaen, *Chem. Eur. J*. **2011**, *17*, 13247-13257.

[26] Q. Lu, K. Liu, H. Zhang, Z. Du, X. Wang, F. Wang, *ACS Nano* **2009**, *3*, 3861-3868.

[27] X. Zhao, C. Huang, M. Gulcur, A. S. Batsanov, M. Baghernejad, W. Hong, M. R. Bryce, T. Wandlowski, *Chem. Mater*. **2013**, 25, 4340-4347.

[28] K. Sonogashira, *J. Organomet. Chem*. **2002**, *653*, 46.

[29] L.O. Pålsson, C. Wang, A.S. Batsanov, S. M. King, A. Beeby, A. P. Monkman, M. R. Bryce, *Chem. Eur. J.* **2010**, *16*, 1470-1479.

[30] C. Wang, L.-O. Pålsson, A. S. Batsanov, M. R. Bryce, *J. Am. Chem. Soc*. **2006**, *128*, 3789-3799.

[31] C. Lambert, G. Nöll, *J. Am. Chem. Soc*. **1999**, *121*, 8434-8442.

[32] A. Rosspeintner, G. Angulo, C. Onitsch, M. Kivala, F. Diederich, G. Grampp, G. Gescheidt, *ChemPhysChem* **2010**, *11*, 1700-1710.

[33] A. C. Benniston, A. Harriman, J. P. Rostron, *Phys. Chem. Chem. Phys*. **2005**, *7*, 3041-3047.

[34] J. C. Collings, S.-Y. Poon, C. Le Droumaguet, M. Charlot, C. Katan, L.-O. Pålsson, A. Beeby, J. A. Mosely, H. M. Kaiser, D. Kaufmann, W.-Y. Wong, M. Blanchard-Desce, T. B. Marder, *Chem. Eur. J*. **2009**, *15*, 198-208.

[35] W. Rettig, *Angew. Chem. Int. Ed. Engl.* **1986**, *25*, 971–988.

[36] J. C. Collings, A. C. Parsons, L. Porrès, A. Beeby, A.S. Batsanov, J. A. K. Howard, D. P. Lydon, P. J. Low, I. J. S. Fairlamb, T. B. Marder, *Chem. Commun*. **2005**, 2666-2668.

[37] L. Weber, D. Eickhoff, T. B. Marder, M. A. Fox, P. J. Low, A. D. Dwyer, D. J. Tozer, S. Schwedler, A. Brockhinke, H.-G. Stammler, B. Neumann, *Chem. Eur. J.* 2012, **18**, 1369-1382.

[38] Y. Yamaguchi, T. Tanaka, S. Kobayashi, T. Wakamiya, Y. Matsubara, Z. Yoshida, *J. Am. Chem. Soc.* **2005**, *127*, 9332-9333.

[39] P. V. James, P. K. Sudeep, C. H. Suresh, K. G. Thomas, *J. Phys. Chem. A* **2006**, *110*, 4329-4337.

[40] N. Santhanamoorthi, K. Senthilkumar, P. Kolandaivel, *Mol. Phys*. **2009**, *107*, 1629-1639.

[41] G. de la Torre, F. Giacalone, J. L. Segura, N. Martín, D. M. Guldi, *Chem. Eur. J.* **2005**, *11*, 1267-1280.

[42] F. Giacalone, J. L. Segura, N. Martín, D. M. Guldi, *J. Am. Chem. Soc.* **2004**, *126*, 5340-5341.

[43] L. Porrès, A. Holland, L-O. Pålsson, A. P. Monkman, C. Kemp, A. Beeby, *J. Fluor.* **2006,** 16, 267-273.

Table of Contents

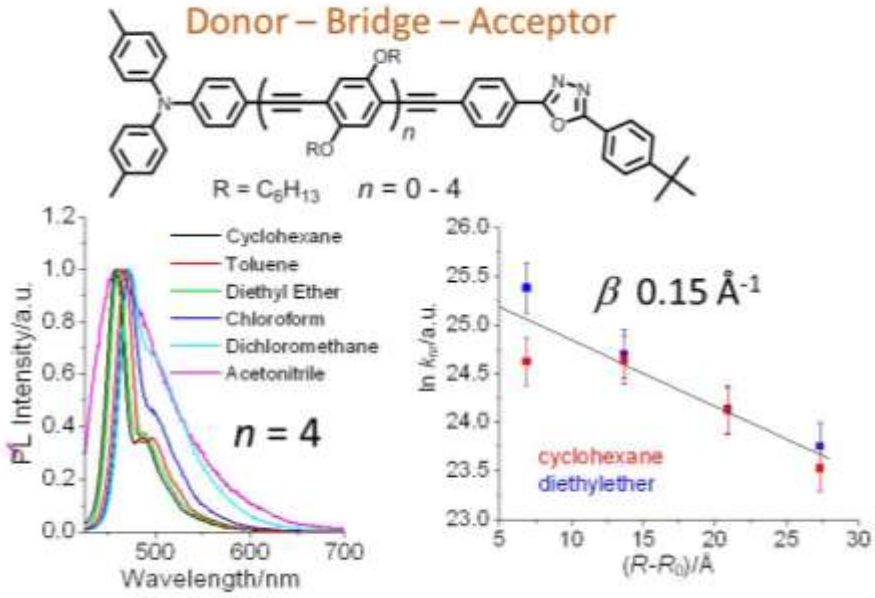

For the series of D–B–A dyads **a**n attenuation factor β of 0.15 $Å^{-1}$ was determined in accordance with an ICT superexchange mechanism.